

Quantum transfer-matrix approach to $S=1$ antiferromagnetic chains at finite temperatures

G. Kamieniarz* and R. Matysiak

Computational Physics Division, Institute of Physics, A. Mickiewicz University, ul. Umultowska 85, 61-614 Poznań, Poland

A. Caramico D'Auria, F. Esposito,[†] and U. Esposito

Dipartimento di Scienze Fisiche, Università di Napoli, Piazzale Tecchio, 80125 Napoli, Italy

(Received 24 June 1996; revised manuscript received 30 January 1997)

The quantum transfer-matrix method (QTM) has been applied to study the finite-temperature static properties of the spin $S=1$ antiferromagnetic Heisenberg chains in a wide range of the single-ion anisotropy and temperatures. The high-resolution QTM simulation data are obtained for the zero-field susceptibility, specific heat, as well as for the field-dependent magnetization. The microscopic parameters of a number of real quasi-one-dimensional compounds are found from fitting procedures, some theoretical approaches are numerically verified and low-temperature extensions of high-temperature series are given in terms of Chebyshev polynomials. [S0163-1829(97)02325-4]

I. INTRODUCTION

Haldane conjecture showing the difference between the ground state of integer and half-integer spins has stimulated a lot of theoretical and experimental interest in antiferromagnetic quantum spins chains. The ground state of integer spin chains was predicted disordered with a gap in the excitation spectrum and the spin-correlation function decaying exponentially. The existence of the gap has been well established by various numerical techniques and field-theoretical arguments. The first experimental evidence for the gap in the excitation spectrum were results of the neutron scattering¹ on CsNiCl_3 although the compound is only moderately one dimensional. A representative physical realization of one-dimensional Heisenberg antiferromagnets (1D-HAF's) is another Ni^{2+} ($S=1$) compound $\text{Ni}(\text{C}_2\text{H}_8\text{N}_2)_2\text{NO}_2\text{ClO}_4$, abbreviated as NENP,² displaying no magnetic long-range order down to very low temperatures. Over the years, other real spin chains with varying anisotropies have been synthesized³⁻⁶ [e.g., $(\text{CH}_3)_4\text{NNi}(\text{NO}_2)_3\text{-TMNIN}$, $\text{Y}_2\text{BaNiO}_5\text{-YBANO}$, AgVP_2S_6 , $\text{Ni}(\text{C}_2\text{H}_8\text{N}_2)_2\text{Ni}(\text{CN})_4\text{-NENC}$] and measurements of susceptibility, field-dependent magnetization, ESR and NMR have been performed. Quantitative interpretation of the experimental results is based on different approximate theories⁴ so that it is subject to some ambiguities. Moreover, the experimental data sometimes are not unique, as can be seen in the case of susceptibility measured for NENP,^{2,7} TMNIN,^{3,8,9} or YBANO.^{4,10,11}

The nature of the Haldane phase still needs some clarification.¹² The peculiar property of the disordered ground state is an antiferromagnetic hidden order described by a nonlocal string order parameter. The integer spin chains with weak anisotropy can be mapped onto the quantum nonlinear σ models¹³ with the bare coupling constant $g_0=2/S$. Particularly for $S=1$ chains, the nonlinear σ model is only valid in a narrow range of temperatures. Apart from the nonlinear σ model, other theories have been developed for the low-temperature static and dynamic properties which include boson or fermion models,¹⁴ self-consistent mean-field¹⁵ or strong-coupling¹⁶ approaches.

The aim of this paper is to verify some theoretical results and the values of the microscopic parameters, earlier selected from different fitting procedures, using reliable numerical simulations based on the unique quantum transfer-matrix technique (QTM).

In the presence of the external field, the 1D HAF chains are described by the $S=1$ Hamiltonian

$$\mathcal{H} = J \sum_{i=1}^{N-1} S_i \cdot S_{i+1} + D \sum_{i=1}^N (S_i^z)^2 - g_\alpha \mu_B B \sum_{i=1}^N S_i^\alpha, \quad (1)$$

where J (>0) denotes the antiferromagnetic interaction constant, D stands for the anisotropy parameter, B is the external magnetic field which can be applied along the chain ($\alpha=z$) or in the perpendicular direction ($\alpha=x$), and g_α is the corresponding gyromagnetic ratio.

A number of simulation techniques^{13,17-22} has been applied to 1D HAF chains. Herein, the variant of the QTM approach proposed by Delica *et al.*¹⁸ has been adapted. Our simulations are performed for a classical counterpart of the model (1) defined on the square lattice consisting of $N \times 2m$ Ising spins, where m is an integer referred to as the Trotter number. The following features of the present transfer-matrix technique are worth noticing: no statistical errors, the real-space decomposition scheme, reduction of the amount of independent configurations to 3^{Nm} and a collapse of all the states under the trace operation onto a single one. This enables the computer runs for chains as long as necessary to establish the leading eigenvectors of the transfer matrix with an accuracy to 10^{-8} and $m=8$.

The remainder of this paper is organized as follows. In the next section we describe briefly our methods of simulation and analysis, we demonstrate the variation of our finite-size data and explain the extrapolation procedure. Our main results are presented in Sec. III and compared to the experimental data on the real 1D HAF compounds and some theoretical predictions. The paper is concluded with some discussion of the results and indications for further applications of our technique.

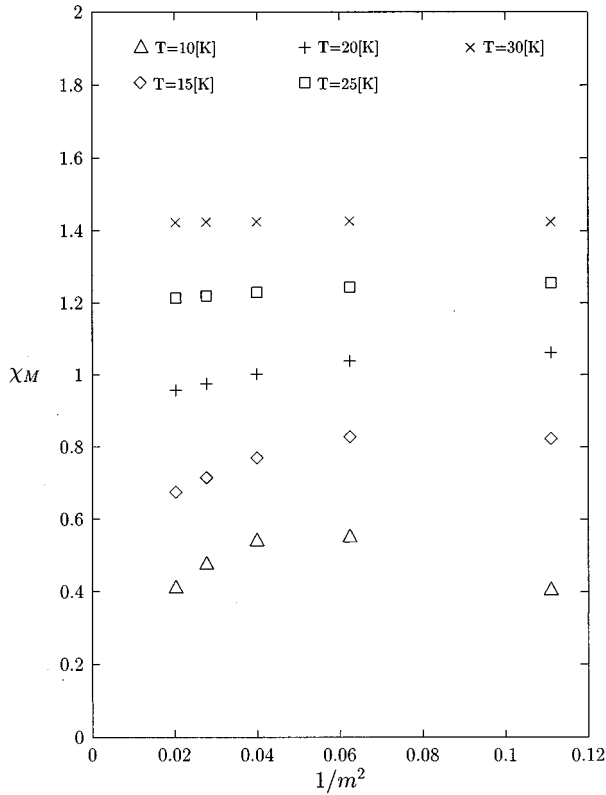


FIG. 1. Variation of the molar susceptibility χ in (m emu/mol) against $1/m^2$ (the transfer-matrix data, $3 \leq m \leq 7$).

II. THE QUANTUM TRANSFER-MATRIX TECHNIQUE

We calculate both the canonical partition function Z , which for the spin system described above (1) can be defined as

$$Z = \text{Tr} e^{-\beta \mathcal{H}},$$

and the thermodynamical mean value of a quantity described by the self-adjoint operator \mathcal{A} which is given by

$$\langle \mathcal{A} \rangle = \frac{1}{Z} \text{Tr} \mathcal{A} e^{-\beta \mathcal{H}}.$$

The values of matrix elements of $e^{-\beta \mathcal{H}}$ cannot be found exactly for large N because of noncommuting operators in \mathcal{H} . Thus, to eliminate this restriction we look for the systematic approximants to functions Z and $\langle \mathcal{A} \rangle$.

For long chains, we rewrite the Hamiltonian (1) in terms of two-site operators

$$\mathcal{H} = \sum_{i=1}^{N-1} \mathcal{H}_{i,i+1}, \quad (2)$$

where

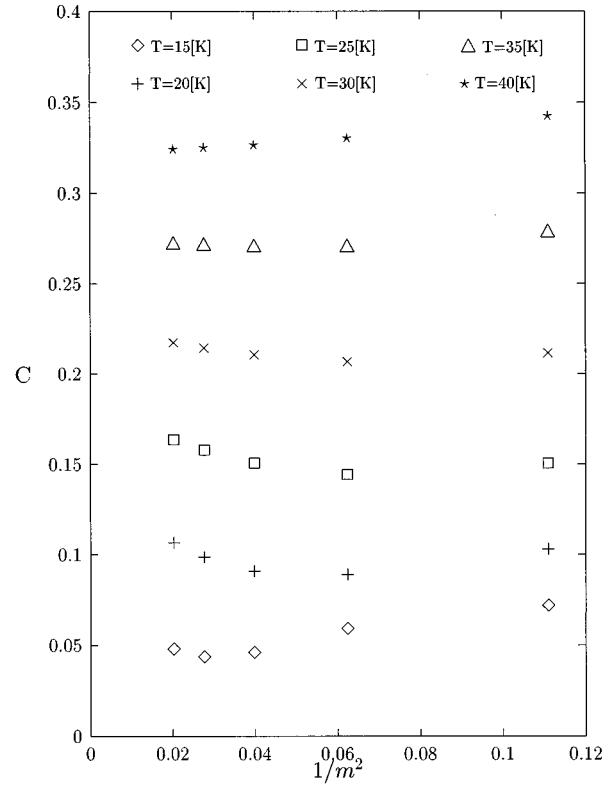


FIG. 2. Variation of the specific heat C per spin against $1/m^2$ (the transfer-matrix data, $3 \leq m \leq 7$).

$$\mathcal{H}_{i,i+1} = J \vec{S}_i \cdot \vec{S}_{i+1} + \frac{1}{2} D [(S_i^z)^2 + (S_{i+1}^z)^2] - \frac{1}{2} g_\alpha \mu B (S_i^\alpha + S_{i+1}^\alpha).$$

By using the general Suzuki-Trotter formula,^{23,24} we introduce the operator

$$\mathcal{R}(\beta) = \prod_{i=1}^{N-1} e^{-\beta \mathcal{H}_{i,i+1}},$$

so that the partition function Z can be evaluated from the equation

$$Z = \lim_{m \rightarrow \infty} Z_m = \lim_{m \rightarrow \infty} \text{Tr} [\mathcal{R}(\beta/m)]^m, \quad (3)$$

TABLE I. The Chebyshev coefficients of the low-temperatures part of the susceptibility χ and the specific heat C .

i	a_i	b_i	i	a_i	b_i
0	0.0798994	0.2504432	6	-0.0049973	-0.0149541
1	-0.0712023	-0.2276052	7	-0.0033515	0.0051486
2	0.0261014	0.0092536	8	-0.0039109	0.0017821
3	-0.0012213	0.0418732	9	-0.0018993	
4	-0.0020003	-0.0510788	10	-0.0011700	
5	-0.0029195	0.0352618			

where m is the natural number (the Trotter number) and the right side presents the m th approximant Z_m to Z in the real-space decomposition²³ defined by Eq. (2). Z_m can be calculated numerically without any restrictions on the value of N by the quantum transfer-matrix method.²³ However, because of computer memory limitations, calculation of Z_m is possible to relatively small values of m (in our case $m \leq 8$). It was shown elsewhere²⁴ that the leading errors in taking a finite m approximants are of the order of $1/m^2$.

The mean value of a quantity represented by operator \mathcal{A} can be approximated by

$$\langle \mathcal{A} \rangle_m = \frac{1}{Z_m} \text{Tr} \mathcal{A} [\mathcal{R}(\beta/m)]^m. \quad (4)$$

The magnetization per site in the α direction is calculated putting in Eq. (4) the α component of the central spin of the chain. The susceptibility can be then calculated by numerical differentiation of magnetization. The specific heat can be obtained as a first derivative of the two-spin correlation function $\langle S_i S_{i+1} \rangle$ and the average $\langle (S_i^z)^2 \rangle$ which are directly related to internal energy.

The numerical implementation of Eqs. (3) and (4) is based on a global transfer operator²³ W acting in the \mathcal{H}^{2m} space which is a direct product of $2m$ single-spin spaces:

$$\mathcal{H}^{2m} \equiv \otimes_{i=1}^{2m} \mathcal{H}_i.$$

In the cited paper it is shown that, putting

$$|a\rangle \equiv \prod_{i=1}^m \delta_{\sigma_{2i-1}, \sigma_{2i}},$$

$$|b\rangle \equiv \prod_{i=1}^m \delta_{\sigma_{2i}, \sigma_{2i}},$$

the m th approximant to the canonical partition function can be written

$$Z_m = \langle b | W^{N-1} | a \rangle, \quad (5)$$

where N is the chain length, and the mean value of the central site spin in the α direction is

$$\langle S_\alpha \rangle_m = \frac{1}{Z_m} \langle b | W^{N-n} S_\alpha W^{n-1} | a \rangle, \quad (6)$$

where S_α is the single-site spin operator and $n = N/2$.

In this paper the QTM technique outlined in our previous work²⁵ has been developed. We have noticed that repeated application of the W operator to the vector $|a\rangle$ ($|b\rangle$), for N big enough, produces an eigenvector of W . The limit of an infinite chain is specified by the matrix element of the spin operator between the left and right eigenvectors. So the criterion for the N value is to iterate the W operator application until a stable eigenvector (within a preset precision) is reached. We found that the N value strongly depends on temperature. For $k_B T$ comparable with the coupling J , $N \approx 20-30$ is sufficient; for $k_B T/J \approx 0.1-0.2$ (the smallest value for which we can confidently extrapolate to $m \rightarrow \infty$) it is necessary to take $N \approx 300-500$.

We performed a comprehensive test of the convergence properties of the QTM approximants to the thermodynamic quantities in our previous work²⁵ on the ferromagnetic CsNiF_3 . We have verified that a similar convergence in terms of $1/m^2$ occurs for the antiferromagnetic model (1). Typical variations of the zero-field susceptibility and specific heat results for various temperatures are presented in Figs. 1 and 2, respectively. In the region of higher temperatures, our estimates show the linear behaviour with respect to $1/m^2$, whereas for lower temperatures some nonlinearities emerge and impose uncertainties on our extrapolations for $m \rightarrow \infty$. In our QTM computations we tune the temperature region so that the uncertainties do not exceed 10%.

III. RESULTS

A. Isotropic limit

High-temperatures series expansion results for susceptibility and specific heat play an important role in interpretation of experimental results on 1D HAF systems. They are even resorted to in the presence of anisotropy^{3,4,26,27} down to $k_B T/J \approx 1$. Unfortunately, in the region of their applicability, the estimates of thermodynamic quantities are rather insensitive to the changes of the microscopic parameters. Thus we have extended QTM numerical calculations down to $k_B T/J \approx 0.1$ and we have found the coefficients of the Chebyshev polynomials in term of $x = J/k_B T$ both for the reduced susceptibility

$$\chi J / N g^2 \mu_\beta^2 = \sum_{i=0}^n a_i T_i(x) \quad (7)$$

and the per site specific heat

$$C / N k_B = \sum_{i=0}^n b_i T_i(x), \quad (8)$$

where $T_n(x)$ denotes the n th order polynomial. The coefficients a_i and b_i have been evaluated from the best fit of our numerical data in the region $0.7 \leq x \leq 7$ (i.e., for χ and C below maximum) and are given in Table I. For temperatures above a maximum of χ and C , our results coincide with those established from high-temperature series²⁶⁻²⁸ and the latter can be resorted to. Our isotropic QTM data for χ and C are given in Figs. 3 and 4 by diamonds and are accompanied by error bars (if they are large enough to be seen in the scale). In Fig. 3, the low-temperature continuation of the Weng expression for χ drawn by the continuous line clearly deviates from our curve. By open circles we have marked the numerical data¹³ extrapolated from finite-chain diagonalization technique with periodic boundary conditions imposed in Eq. (1). The experimental susceptibility measurements on TMNIN (Ref. 3) and AgVP_2S_6 (Ref. 5) are also shown in Fig. 3 by filled circles and asterisks, respectively. These two compounds are found isotropic realizations of 1D HAF chains. We demonstrate in Fig. 3 that in low temperatures the experimental results slightly deviate from the pure isotropic behaviour following from our computations.

As to the specific heat shown in Fig. 4, we find a consistency both with the numerical results previously reported²⁹ (the squares) and those for TMNIN (the crosses).

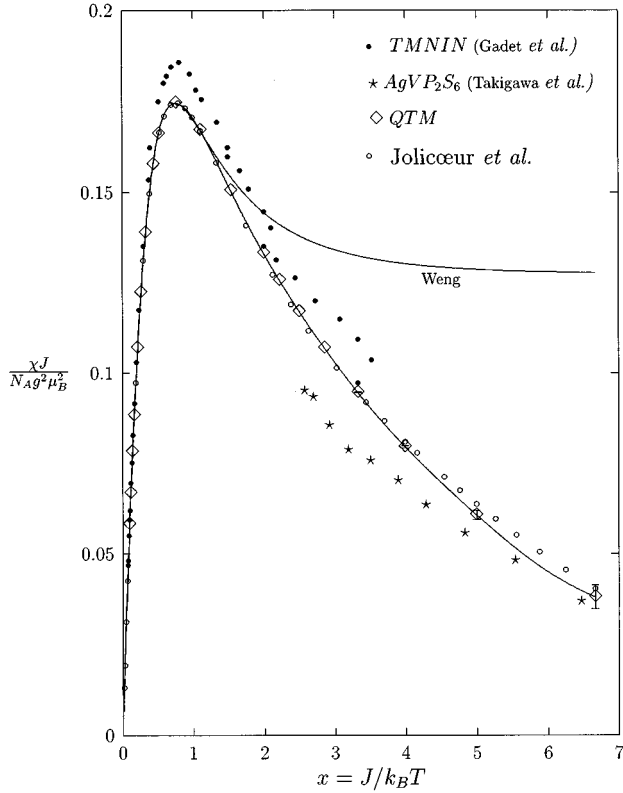


FIG. 3. The isotropic susceptibility in reduced units $Ng^2\mu^2/J$ vs the inverse temperature. The continuous curve fits the numerical QTM results. The remaining symbols represent the experimental and other theoretical data, as labeled.

Our calculations of the zero-field susceptibility and specific heat for TMNIN have been performed with $D=0$, $g=2.25$, and $J/k_B=12$ K, as found in literature.³ Using the same values of the interactions parameters, we have carried out simulations in the presence of an external field which yielded the magnetization profiles at constant temperatures ($T=1.9$ K and $T=15$ K) drawn in Fig. 5. For the isotherm at the 1.9 K, the accuracy for our estimates is of the order of 10% and for that at $T=15$ K—about 1%. The experimental findings for TMNIN (Ref. 3) are plotted both by the lines (to guide eyes) and by the symbols described by the labels. Our QTM data agree with experiment, although in higher fields display a tendency to go upwards.

In addition, the gap $\Delta/J=0.38\pm 0.04$ has been extracted from our low-temperature ($T=1.9$ K) magnetization curve and agrees within the error bars with the known value 0.41 for the isotropic Hamiltonian. We have followed the idea described by Gadet *et al.*³

B. Moderate anisotropy

We have performed extensive simulations of the model (1) for the parameters spread over the interval previously found for NENP. In particular, we have confirmed the excellent fit of the susceptibility data of Renard *et al.*² for the parameters selected by Delica *et al.*,¹⁸ but we have revealed then pronounced systematic deviations for the magnetization

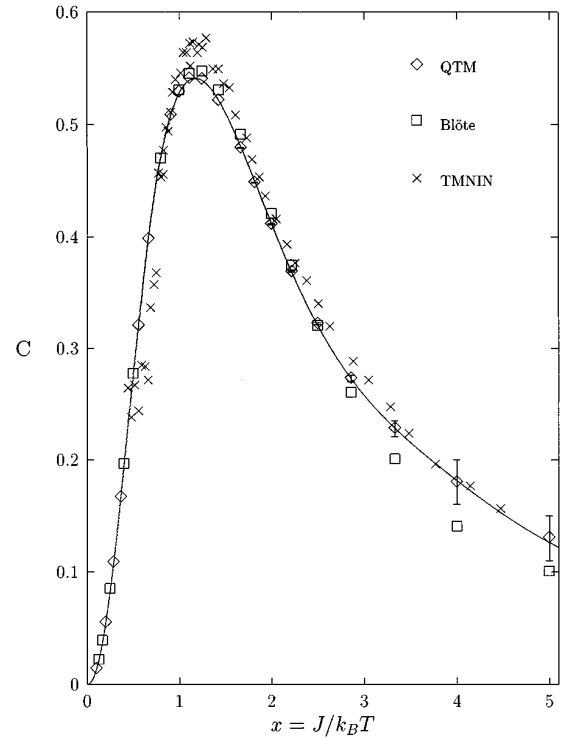


FIG. 4. The isotropic specific heat per spin. The continuous curve fits the numerical QTM data. The remaining symbols represent the experimental and other theoretical data, as described in the legend.

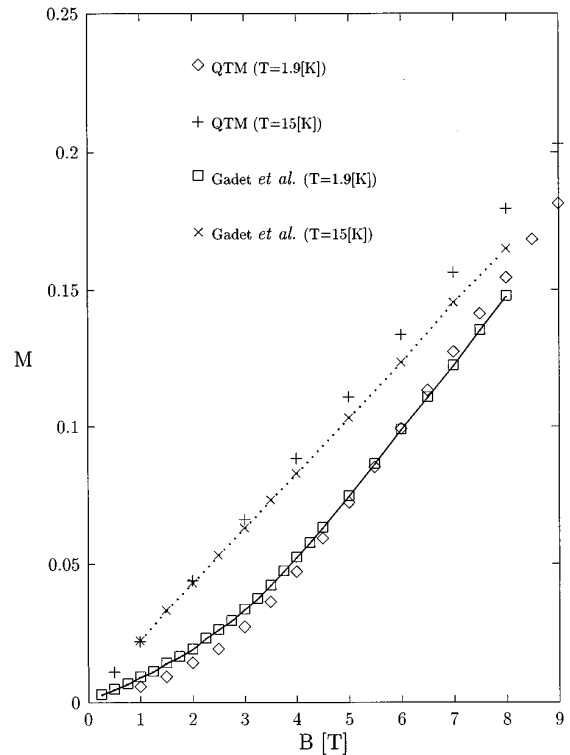


FIG. 5. The field-dependent magnetization data per site and μ_B for TMNIN. The QTM estimates are shown by the symbols only. The experimental results are given by symbols and lines. The symbols are defined in the legend.

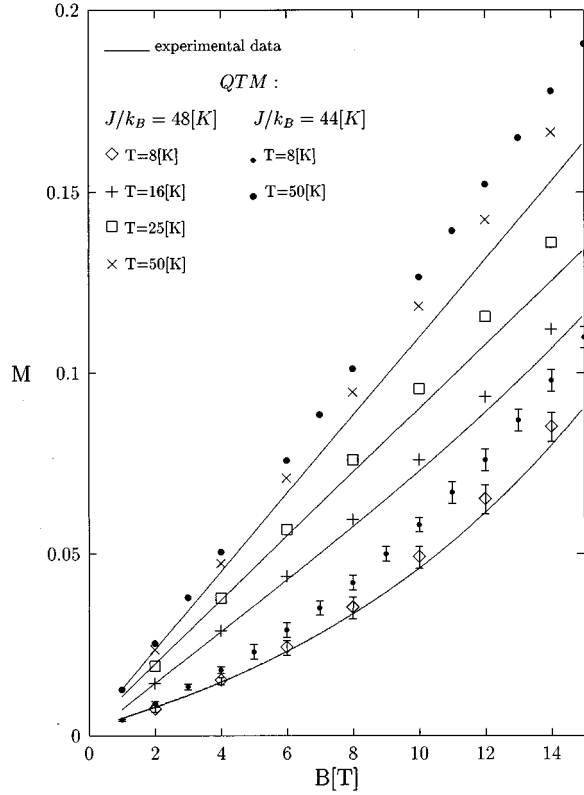


FIG. 6. The magnetization profiles per site and μ_B for NENP against the external field. The QTM data for $J/k_B=48$ K and $J/k_B=44$ K are illustrated by the corresponding symbols and the experimental data are drawn by the continuous lines.

profiles as shown in Fig. 6 by filled circles. As to NENP, we have concluded that the best overall fit can be achieved for the set

$$J/k_B=48 \text{ K}, \quad D/k_B=7.8 \text{ K}, \quad g_{\perp}=2.25, \quad g_{\parallel}=2.20 \quad (9)$$

which is consistent with other estimates existing in literature.^{2,7,18,30}

The results for NENP are illustrated in five figures. In Fig. 6 we display the low-field powder magnetization data both calculated here for the parameters (9) and measured experimentally.² The QTM results are given by the symbols and the experimental findings are drawn by the continuous lines. Extending our computations up to 40 T, also the high-field single-crystal magnetization measurements³⁰ can be reproduced within the error bars. The magnetization isotherms at $T=4.2$ K are shown in Figs. 7 and 8 for the field applied along the chain and in the perpendicular direction, respectively. The symbols with the error bars represent our QTM estimates, whereas the continuous lines follow from the high-field experiments.³⁰ As shown in Fig. 9, the single-crystal zero-field susceptibilities, evaluated for the same parameters, remain consistent with the experimental findings. Our results near the maximum are systematically lower than

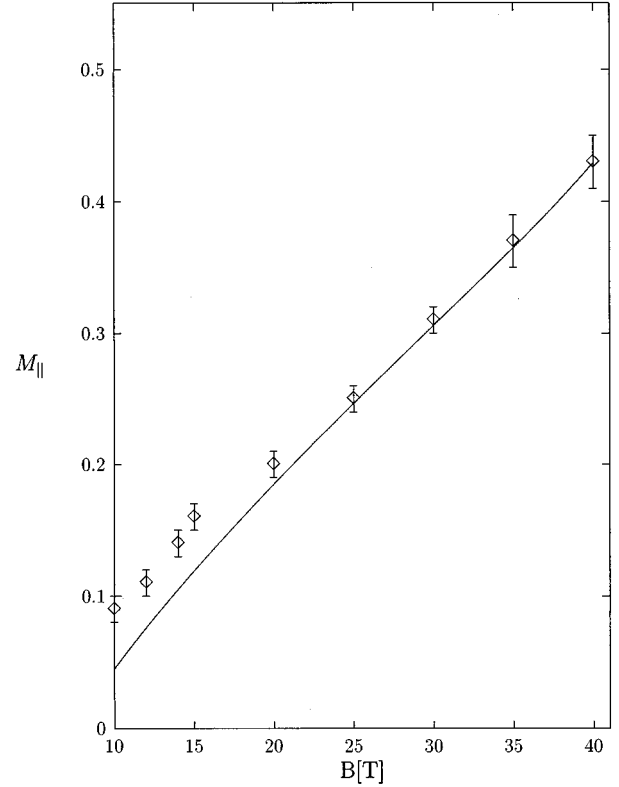


FIG. 7. The large-field dependence of the longitudinal magnetization M_{\parallel} data (per site and μ_B) for NENP [$J/k_B=48$ (K); $T=4.2$ (K)]. Numerical data are shown by the symbols and the experimental results by the lines (Ajiro *et al.*).

those of Renard *et al.*² but some reduction is expected from other measurements,⁷ as shown in Fig. 9.

As to CsNiCl_3 , the estimates of the microscopic parameters deduced from the neutron scattering experiments¹ ($J/k_B=33.2$ K) have been challenged on the basis of the static measurements^{19,31} leading, unfortunately, to inconsistent predictions for the parameters in Eq. (1). Selecting the values of parameters ($J/k_B=27$ K) estimated from the finite-chain data,¹⁹ we have revealed again an agreement between the susceptibility and specific heat results and the corresponding measurements on CsNiCl_3 , whereas our new results coincide with the previous ones¹⁹ within the error bars. The zero-field single-crystal susceptibility data and those for the specific heat are given in Figs. 10 and 11, respectively. Choosing $J/k_B=30$ K, the susceptibility curve (Fig. 11) deviates from the experiment on CsNiCl_3 and the discrepancy would increase for $J/k_B=33.2$ K. However, we cannot discriminate between competing sets of parameters which originate from the static measurements as the magnetization experiment³¹ has been performed in temperatures inaccessible for our simulations.

YBANO is an important compound for investigation of the effects of paramagnetic impurities and spin-1/2 degrees of freedom.³² Although insulating in the absence of impurities, after acceptor doping it belongs to a small group of effective 1D conductors.³³ It is also interesting that some NMR measurements¹¹ performed on YBANO have revealed discrepancies with the existing theory³⁴ of the spin suscepti-

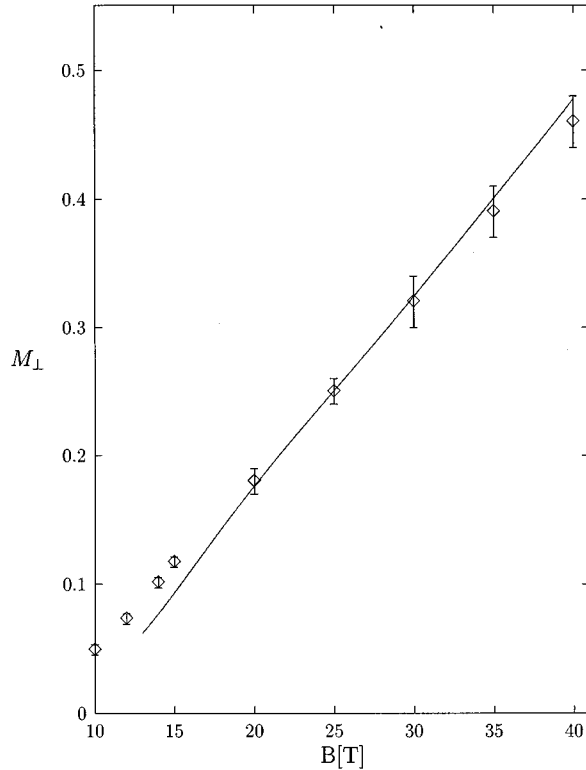


FIG. 8. The large-field dependence of the perpendicular magnetization M_{\perp} data (per site and μ_B) for NENP [$J/k_B=48$ (K); $T=4.2$ (K)]. Numerical data are shown by the symbols and the experimental results by the lines (Ajiro *et al.*).

bility in the Haldane-gap antiferromagnets. In Fig. 12 we have presented the experimental values of the zero-field susceptibility as found by different techniques^{4,10,11} and we have fitted these data within the model (1). We have extended the fit down to $T=40$ K which was not accessible before.⁴ For lower temperatures we have considered the classical systems up to $m=8$ and receiving the curve drawn by the continuous line in Fig. 12. Our final outcome is consistent with the experimental data. However, it was rather difficult to reach agreement in the low-temperature part of the susceptibility. From our simulations we have established the following set of the microscopic parameters:

$$J/k_B=275 \text{ K}, \quad D/k_B=60 \text{ K}, \quad g=2.33. \quad (10)$$

Numerical simulations are valuable tools for testing approximate analytical approaches. As to the anisotropic 1D HAF systems, theoretical boson and fermion models have been adopted.¹⁴ The appropriate predictions have been found in the region accessible for reliable numerical computations, assuming the following parameters:

$$J/k_B=46 \text{ K}, \quad D/J=0.16,$$

close to those for NENP. In our simulations, we have put $g_{\perp}=2.22$ (or 2.20), $g_{\parallel}=2.15$ (which are not specified by Regnault *et al.*) and we have revealed pronounced discrepancies in the behavior of both susceptibility and specific heat. In Fig. 13 the single-crystal susceptibility data are illustrated in the reduced units ($Ng^2\mu^2/J$). The theoretical

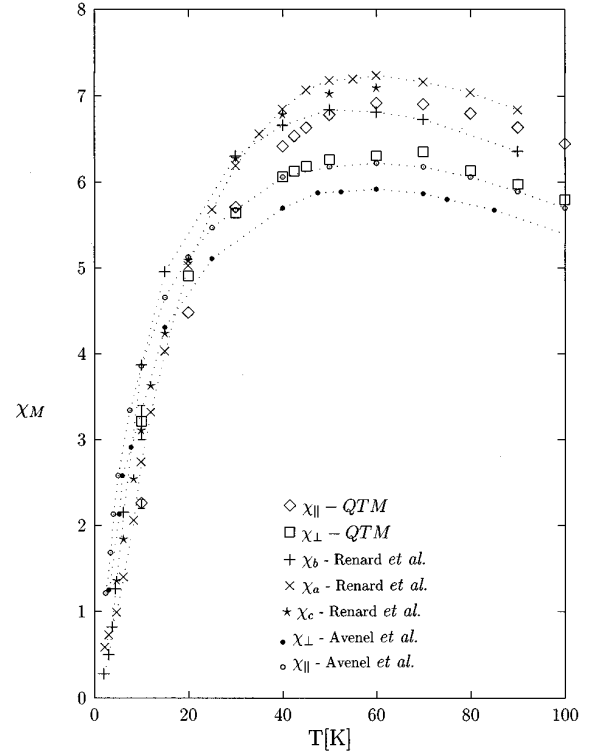


FIG. 9. The temperature behavior of the single-crystal molar susceptibility for NENP in (m emu/mol). The experimental results are guided by the dotted lines.

predictions are plotted by continuous and dotted lines for the boson and fermion models, respectively, whereas the corresponding QTM numerical estimates are drawn by the symbols. The bold line and the tight dotted curve in Fig. 13 refer to the calculations carried out in the hard direction parallel to the chain. The remaining continuous and dotted lines refer to the theoretical estimates in the perpendicular direction. The circles in Fig. 13 represent results of some quantum Monte Carlo calculations,^{14,22} which agree within the error bars with our QTM estimates for $k_B T/J \leq 0.2$. The temperature dependence of the specific heat per spin is illustrated in Fig. 14. The theoretical results are drawn by continuous lines and the measured values in the region of very low temperatures are shown by crosses. Our QTM estimates follow a curve lying between that of the fermion and the boson model.

C. Strong anisotropy limit

We consider here the strong anisotropy $D/J=7.5$, to test a perturbational theoretical approach applied to obtain the parameters for NENC.¹⁶ Our results for the zero-field single-crystal susceptibility and specific heat are consistent with those coming from the analytical calculations. This is demonstrated in Figs. 15 and 16, where our estimates given by the symbols are compared with the corresponding theoretical predictions¹⁶ drawn by the continuous lines. We detect only minor deviations in the low-temperature behavior of χ_{\perp} .

IV. CONCLUSIONS

We have carried out large-scale computations obtaining high resolution data for the $S=1$ antiferromagnetic chains

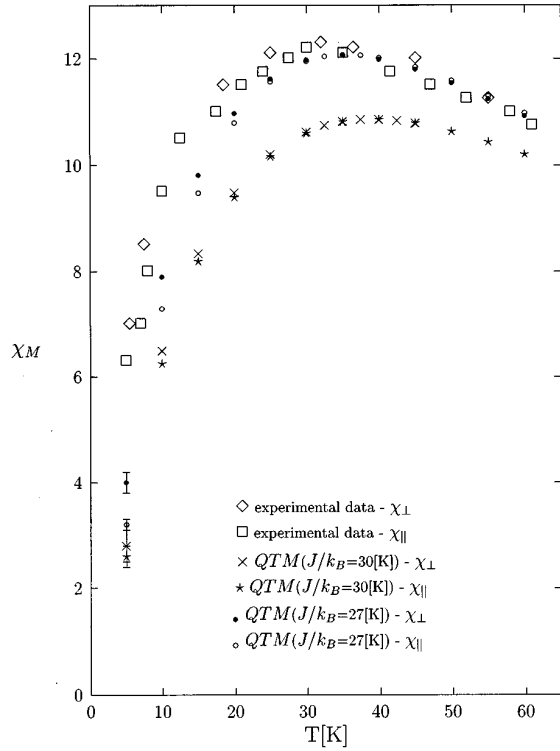


FIG. 10. The temperature dependence of the molar susceptibility for CsNiCl_3 in (m emu/mol). The numerical and experimental data are illustrated by the symbols as labeled.

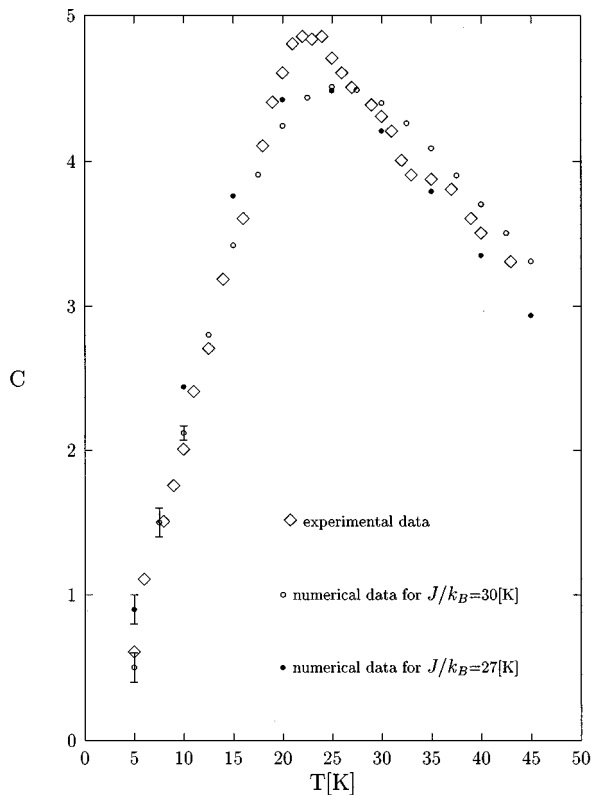


FIG. 11. The temperature dependence of the specific heat per spin for CsNiCl_3 calculated numerically and found experimentally.

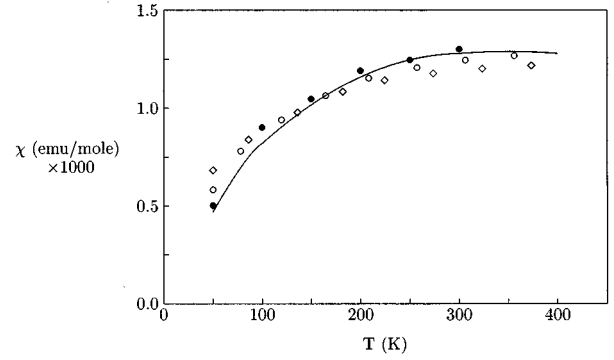


FIG. 12. Temperature dependence of the susceptibility χ for YBANO. The full line illustrates the QTM estimates. The experimental data are given as follows: (\diamond) Darriet *et al.*; (\circ) Batlogg *et al.*; (\bullet) Shimizu *et al.*

down to low temperatures. The parameters (9) and (10) have been established as the best sets describing static measurements for NENP and YBANO. In the case of TMNIN and AgVP_2S_6 , slight deviations from the purely isotropic behavior of magnetization and susceptibility have been noted. We have calculated low-temperature extensions of the known high-temperature series^{4,27} suitable for the interpretation of the isotropic susceptibility and the specific heat data. Finally, some numerical tests of the recently developed theories have also been carried out.

As to the reliability of our QTM technique, it is applicable

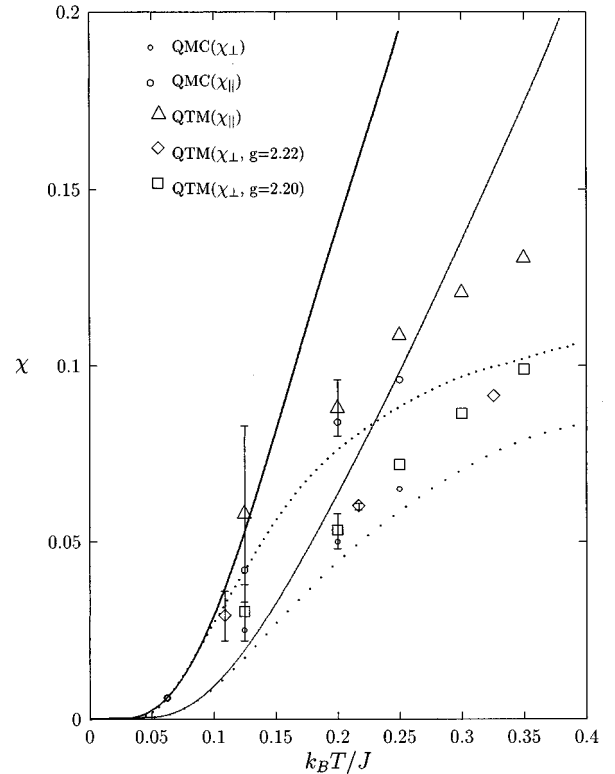


FIG. 13. A comparison between numerical and theoretical predictions for the temperature dependence of the anisotropic susceptibility per spin. The boson and fermion approximations yield continuous lines and dotted lines, respectively. The symbols represent the numerical QTM and QMC estimates and are self-defined.

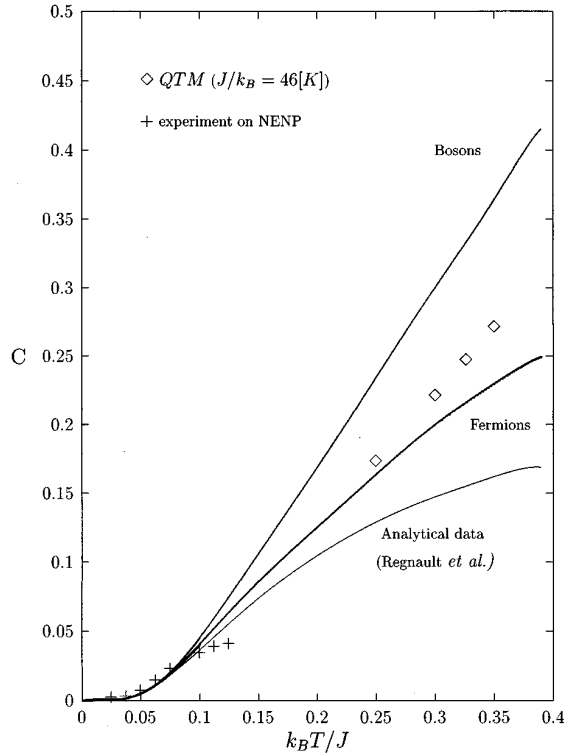


FIG. 14. A comparison between the QTM numerical estimates and those found theoretically and experimentally on NENP for the temperature dependence of the specific heat per spin.

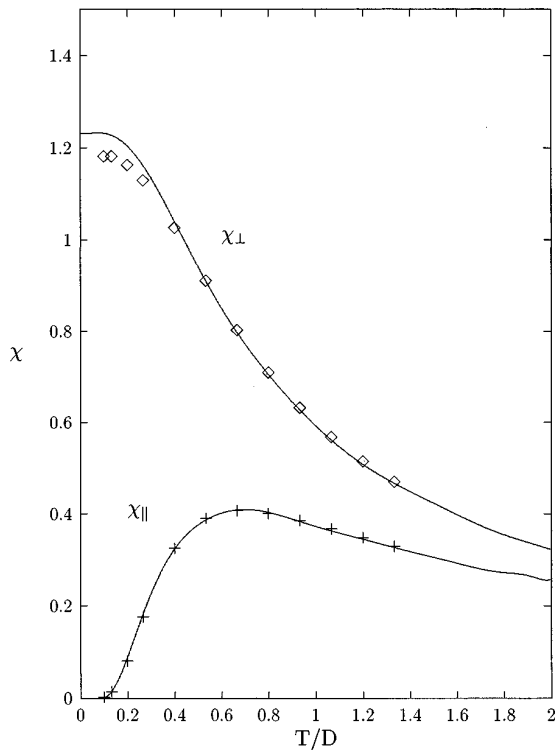


FIG. 15. The temperature dependence of the susceptibility in the limit of the strong anisotropy $D/J=7.5$. The symbols illustrate our results and the continuous curves the corresponding theoretical findings in units $Ng^2\mu_B^2/D$.

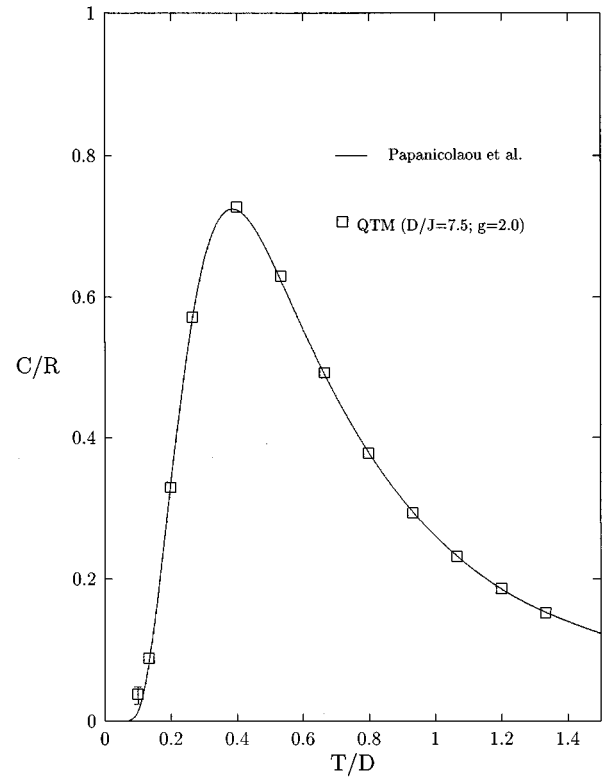


FIG. 16. The temperature dependence of the specific heat in the limit of the strong anisotropy $D/J=7.5$. The symbols illustrate our results and the continuous curves the corresponding theoretical findings.

in the whole region of the microscopic parameters and for temperatures down to $k_B T/J \approx 0.1$. Our simulation data are provided with the error bar estimates if they exceed the size of the symbols, and the convergence of the numerical results in terms of $1/m^2$ is carefully checked. Typical variation of the data (Figs. 1 and 2) is similar to that reported for the ferromagnetic chains.²⁵ For the lower temperatures uncertainties of our extrapolation $1/m^2$ are of the order of 10% and are significantly diminished for higher temperatures.

Our simulations demonstrate that the QTM approach is a valuable tool for calculations of the finite-temperature properties of the Haldane-gap systems. This approach is also expected to be effective for some metallo-organic and mesoscopic one-dimensional compounds.

ACKNOWLEDGMENTS

We would like to thank Professor J. P. Renard for some clarifying discussions and M. Bieliński and L. Dębski for their technical assistance. This work was supported in part by Committee for Scientific Research under the KBN Grant No. 2 P302 116 06. The numerical calculations were carried out on Cray J916 in the Supercomputing and Networking Center in Poznań.

- *Electronic address: gjk@phys.amu.edu.pl
†Electronic address: filesip@osfna1.na.infn.it
- ¹R. M. Morra, W. Buyers, R. Armstrong, and K. Hirakawa, *Phys. Rev. B* **38**, 543 (1989).
 - ²J. P. Renard, M. Verdagner, L. P. Regnault, W. A. C. Erkelens, J. Rossat-Mignad, J. Ribas, W. G. Stirling, and C. Vettier, *J. Appl. Phys.* **63**, 3538 (1988).
 - ³V. Gadet, M. Verdagner, V. Briois, A. Gleizes, J. P. Renard, P. Beauvillain, C. Chappert, T. Goto, K. Le Dang, and P. Veillet, *Phys. Rev. B* **44**, 705 (1991).
 - ⁴J. Darriet and L. P. Regnault, *Solid State Commun.* **86**, 409 (1993).
 - ⁵T. Asano, Y. Ajiro, M. Mutka, H. Yamazaki, N. Hosoi, T. Shinjo, and H. Kikuchi, *Solid State Commun.* **90**, 125 (1994).
 - ⁶M. Orendáč, A. Orendáčová, J. Černák, A. Feher, P. J. C. Signore, M. W. Meisel, S. Merah, and M. Vardagner, *Phys. Rev. B* **52**, 3435 (1995).
 - ⁷O. Avenel, J. Xu, J. S. Xia, M-F. Xu, B. Andraka, T. Lang, P. L. Moyland, W. Ni, P. J. C. Signore, C. M. C. M. van Woerkens, E. D. Adams, G. G. Ihas, M. W. Meisel, S. E. Nagler, N. S. Sullivan, Y. Takano, D. R. Talham, T. Goto, and N. Fujiwara, *Phys. Rev. B* **46**, 8655 (1992).
 - ⁸L.-K. Chou, K. A. Abboud, D. R. Talham, W. W. Kim, and M. W. Meisel, *Physica B* **194-196**, 311 (1994).
 - ⁹M. Ito, M. Mito, H. Deguchi, and K. Takeda, *J. Phys. Soc. Jpn.* **63**, 1123 (1994).
 - ¹⁰S. Batlogg, S.-W. Cheong, and L. W. Rupp, Jr., *Physica B* **194-196**, 173 (1994).
 - ¹¹T. Shimizu, D. E. MacLaughlin, P. C. Hammel, J. D. Thompson, and S.-W. Cheong, *Phys. Rev. B* **52**, R9835 (1995).
 - ¹²H. J. Mikeska and P. Verrucchi, *Phys. Rev. B* **52**, 3571 (1995).
 - ¹³Th. Jolicœur and O. Golinelli, *Phys. Rev. B* **50**, 9265 (1994).
 - ¹⁴L. P. Regnault, I. Zaliznyak, and S. Meshkov, *J. Phys. Condens. Matter* **5**, L677 (1993).
 - ¹⁵H.-T. Wang, J.-L. Shen, K.-R. Li, and Z.-B. Su, *Phys. Rev. B* **51**, 16 103 (1995).
 - ¹⁶N. Papanicolaou and P. N. Spathis, *Phys. Rev. B* **52**, 16 001 (1995).
 - ¹⁷A. Furusaki, M. Sigrist, E. Westerberg, P. A. Lee, K. B. Tanaka, and N. Nagaosa, *Phys. Rev. B* **52**, 15 930 (1995).
 - ¹⁸T. Delica, K. Kopinga, H. Leshke, and K. K. Mon, *Europhys. Lett.* **15**, 55 (1991).
 - ¹⁹L. S. Campana, A. Caramico D'Auria, F. Esposito, U. Esposito, and G. Kamieniarz, *Phys. Rev. B* **45**, 5035 (1992).
 - ²⁰S. Yamamoto and S. Miyashita, *Phys. Rev. B* **48**, 9528 (1993).
 - ²¹S. Yamamoto and S. Miyashita, *Phys. Rev. B* **50**, 6277 (1994).
 - ²²S. V. Meshkov, *Phys. Rev. B* **48**, 6167 (1993).
 - ²³T. Delica and H. Leshke, *Physica A* **168**, 736 (1990).
 - ²⁴M. Suzuki, *Phys. Rev. B* **31**, 2957 (1985).
 - ²⁵L. S. Campana, A. Caramico D'Auria, F. Esposito, U. Esposito, and G. Kamieniarz, *Phys. Rev. B* **53**, 2594 (1996).
 - ²⁶C. Y. Weng, Ph.D. thesis, Carnegie Institute of Technology, 1968.
 - ²⁷T. de Neef, *Phys. Rev. B* **13**, 4141 (1976).
 - ²⁸M. Takigawa, T. Asano, Y. Ajiro, and M. Mekata, *Phys. Rev. B* **52**, R13 087 (1995).
 - ²⁹H. W. J. Blöte, *Physica B* **79**, 427 (1975).
 - ³⁰Y. Ajiro, T. Goto, H. Kikuchi, T. Sakakibara, and T. Inami, *Phys. Rev. Lett.* **63**, 1424 (1989).
 - ³¹M. E. Zhitomirsky and I. A. Zaliznyak, *Phys. Rev. B* **53**, 3428 (1996).
 - ³²A. P. Ramirez, S.-W. Cheong, and M. L. Kaplan, *Phys. Rev. Lett.* **72**, 3108 (1994).
 - ³³J. F. DiTusa, S.-W. Cheong, J.-H. Park, G. Aeppli, C. Broholm, and C. T. Chen, *Phys. Rev. Lett.* **73**, 1857 (1994).
 - ³⁴I. Affleck, *Phys. Rev. B* **41**, 6697 (1990).